Topography of histone H3–H4 interaction with the Hat1–Hat2 acetyltransferase complex

Ye Yue,[1,2,4] Wen-Si Yang,[1,4] Lin Zhang,[1,3] Chao-Pei Liu,[1] and Rui-Ming Xu[1,2]

[1]National Laboratory of Biomacromolecules, Institute of Biophysics, Chinese Academy of Sciences, Beijing 100101, China; [2]University of Chinese Academy of Sciences, Beijing 100049, China

Chaperones influence histone conformation and intermolecular interaction in multiprotein complexes, and the structures obtained with full-length histones often provide more accurate and comprehensive views. Here, our structure of the Hat1–Hat2 acetyltransferase complex bound to Asf1–H3–H4 shows that the core domains of H3 and H4 are involved in binding Hat1 and Hat2, and the N-terminal tail of H3 makes extensive interaction with Hat2. These findings expand the knowledge about histone–protein interaction and implicate a function of Hat2/RbAp46/48, which is a versatile histone chaperone found in many chromatin-associated complexes, in the passing of histones between chaperones.

Supplemental material is available for this article.

Received October 10, 2021; revised version accepted March 14, 2022.

Histone lysine acetylation is a major type of histone modification catalyzed by a family of enzymes known as histone acetyltransferases (HATs) (Roth et al. 2001). These enzymes transfer the acetyl group from acetyl-CoA onto the ε-amino group of specific lysine residues on histones. Following the initial discovery of HAT activities in *Tetrahymena* Gcn5 and yeast Hat1 (Kleff et al. 1995; Brownell et al. 1996; Parthun et al. 1996), more than a dozen different HAT proteins have been identified and characterized, giving rise to detailed mechanistic understandings of HATs (Berndsen and Denu 2008; Marmorstein and Trievel 2009). However, certain aspects of HAT–histone interaction, such as that important for regulation of enzymatic activity and enzymatic activity-independent functions, are less well understood, especially in cases involving large, multidomain HATs; multiprotein HAT complexes; and/or multiprotein substrate complexes, such as the Gcn5-containing SAGA complex (Grant et al. 1997; Sterner et al. 2002; Soffers and Workman 2020; Wang et al. 2020) and the Rtt109–Asf1–H3–H4 H3K56 HAT–substrate complex (Tyler et al. 1999; Driscoll et al. 2007; Han et al. 2007; Zhang et al. 2018).

[*Keywords*: histones; acetyltransferase; structure; enzymatic activity; histone chaperone]

[3]Present address: Department of Molecular and Cell Biology, University of California at Berkeley, Berkeley, CA 94720, USA.
[4]These authors contributed equally to this work.
Corresponding authors: rmxu@ibp.ac.cn

Article published online ahead of print. Article and publication date are online at http://www.genesdev.org/cgi/doi/10.1101/gad.349099.121.

Here we focus our attention on the Hat1–Hat2 acetyltransferase complex, where Hat1 is one of the earliest discovered HATs, and Hat2 (RbAp46/48) is a histone-binding WD40 repeat protein found in numerous multiprotein complexes associated with chromatin processes (Qian et al. 1993; Kleff et al. 1995; Parthun et al. 1996; Verreault et al. 1998). The Hat1–Hat2 complex was originally isolated as a major cytoplasmic histone H4 acetylase, consistent with being a type B HAT (HAT-B) (Parthun et al. 1996; Ruiz-García et al. 1998; Ai and Parthun 2004). The HAT complex primarily acetylates lysine 12 of histone H4 (H4K12), while Hat1 can also acetylate H4K5. The Hat2 subunit has been shown to increase both the HAT activity and the specificity toward H4K12. A nuclear Hat1 complex, termed NuB4, also includes histone chaperone Hif1/NASP (Ai and Parthun 2004; Poveda et al. 2004). Both the cytoplasmic and the nuclear Hat1 complexes appear to acetylate predeposited histones and have been implicated in various pathways of chromatin assembly (Ruiz-García et al. 1998; Verreault et al. 1998). In addition to Hif1, histone chaperone Asf1 has also been shown to associate with Hat1–Hat2 and HAT-B/NuB4 complexes (Qin and Parthun 2002; Campos et al. 2010; Alvarez et al. 2011; Haigney et al. 2015). Asf1 is well known for binding an H3–H4 heterodimer to facilitate nucleosome assembly in both DNA replication-dependent and -independent processes (Mousson et al. 2007).

To date, several structures of Hat1 or Hat1–Hat2 alone or in complex with histone peptides have been determined (Dutnall et al. 1998; Wu et al. 2012; Li et al. 2014). However, compelling evidence suggests that additional structural information is needed to fully account for the biochemical properties of the Hat1–Hat2 complex (Haigney et al. 2015). Furthermore, how the NuB4 complex facilitates the transfer of the H3–H4 complex to Asf1 remains unknown. Here, our structure of yeast Hat1–Hat2 in complex with Asf1–H3–H4 reveals a new binding mode of the N-terminal helix (αN) of H4 to Hat2 and extensive interactions between the N-terminal region of H3 and Hat2, implicating a mechanism of transfer of H3–H4 from Hif1/NASP to Asf1.

Results and Discussion

Overall structure

To gain an overall picture of histones H3–H4 binding to Hat1–Hat2, we assembled a Hat1–Hat2–Asf1–H3–H4 complex using a bacterially expressed, catalytically active fragment of yeast Hat1 (Hat1ΔC, residues 1–320); insect cell-expressed, full-length yeast Hat2; and a separately prepared Asf1–H3–H4 complex using the conserved core of *Aspergillus fumigatus* Asf1 (*Af*Asf1, residues 1–154). *Af*Asf1 was chosen over *Saccharomyces cerevisiae* Asf1 (*Sc*Asf1) because the *Sc*Asf1–H3–H4 complex easily precipitates at low salt concentrations, limiting the ability of its biochemical characterizations only at

a salt concentration much higher than a physiological one (Haigney et al. 2015), while the *Af*Asf1 complex can sustain a salt concentration as low as 150 mM (Zhang et al. 2018). Furthermore, yeast Hat1–Hat2 acetylates *Af*Asf1–H3–H4 and *Sc*Asf1–H3–H4 with nearly identical efficiency, and Hat2 stimulates H4K12 acetylation of *Af*Asf1–H3–H4 by Hat1 in a manner similar to that of *Sc*Asf1 (Supplemental Fig. S1A,B; Haigney et al. 2015). To improve the crystal quality, we removed six N-terminal residues of histone H4 in our sample due to the following considerations: First, H4K5 is a minor Hat1–Hat2 acetylation site, and deleting the first six residues should limit the binding of only H4K12 to the active site of Hat1–Hat2, thus yielding a homogenous sample suitable for structural studies. Second, previous structural studies of human Hat1 and yeast Hat1–Hat2 all used H4 peptides with an authentic N terminus, but the very N-terminal four and six residues were disordered, respectively (Wu et al. 2012; Li et al. 2014). Moreover, the visible H4 residues 4–6 in the human Hat1 complex are not interacting with the enzyme.

Best diffracting crystals were obtained with N-terminal BRIL (cytochrome b_{562}RIL)-fused Hat1ΔC, which was engineered with the intention of optimizing crystal packing (Chun et al. 2012). The 3.3-Å structure of yeast Hat1ΔC–Hat2 bound to the *Af*Asf1(1–154)–H3–H4(7–102) complex and CoA shows an equimolar complex with one molecule each (Fig. 1). Continuous and well-defined densities for residues 8–318 of Hat1, 8–86 and 107–387 of Hat2, 1–14 and 52–134 of H3, 8–100 of H4, and 1–154 of Asf1 were observed. The disordered loop segments in Hat2 (residues 87–106) and H3 (residues 15–51) are surface exposed. Most of the amino acid side chains are well defined, except for some of the solvent-exposed residues. There is no obvious density for BRIL, but it was projected to occupy an empty region near Asf1 in a neighboring complex from crystal packing. A disordered BRIL tag indicates that its fusion did not interfere with the folding or intermolecular interactions of the protein complex. The structural model has been refined to satisfactory statistics and good stereochemistry (Supplemental Table S1).

The structures of Hat1 alone and its complex with Hat2 have been reported previously, and the structure of our Hat1–Hat2 unit agrees with them well (Dutnall et al. 1998; Li et al. 2014). Briefly, Hat1 is an elongated α/β structure composed of an N-terminal and C-terminal domain. The HAT active site is located in the C-terminal domain, which can be further separated into two structural modules, a central α/β-fold module with an extended β sheet of six antiparallel strands sandwiched by an α helix on either side of the β sheet, and an all α-helical C-terminal module that holds the α/β-fold module together with the N-terminal domain from opposite directions (Fig. 1A). The structure of Hat1 in the complex can be superimposed with that of apo Hat1 (PDB: 1BOB) with a RMSD of 0.8 Å. The only major difference is that the Hat2-binding loop (residues 197–210), termed LP1, becomes ordered in the complex structure (Li et al. 2014). Hat2 is a WD40 repeat protein with a seven-bladed β-propeller structure, and it interacts with LP1 of Hat1 principally via amino acid residues located in the β1–β2 and β3–β4 turn regions of the fifth blade (Fig. 1B). Additionally, residues in the loop connecting β3 and β4 (residues 325–342), termed LP2, in the sixth blade of Hat2 also contribute to the interaction with Hat1 (Fig. 1). LP2 protrudes from the outer edge of the β propeller and rests next to the central α/β-fold module of Hat1. The juxtaposition of Hat1 and Hat2 forms a narrow cleft between them, and the N-terminal tail of histone H4 (residues 8–17) is bound in the cleft (Fig. 1).

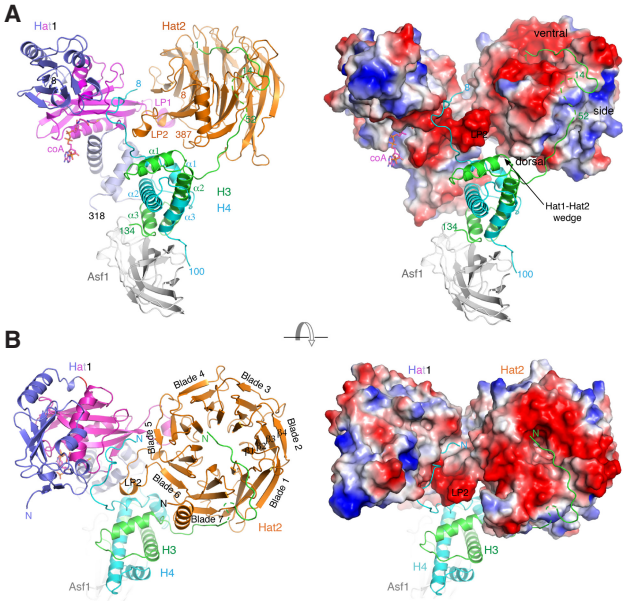

Figure 1. Overall structure. (*A*) A side view of the structure. (*Left* panel) A cartoon representation. The N-terminal domain and the C-terminal helical module of Hat1 are colored slate and light blue, respectively, while the catalytic α/β module is colored magenta; Hat2 is colored orange; histone H3 and H4 are colored green and cyan, respectively; and Asf1 is colored gray. The CoA molecule is shown in a stick model. (*Right* panel) Hat1 and Hat2 are shown in a surface representation colored according to electrostatic potential. (Red) Negative, (white) neutral, (blue) positive. The narrower and wider surface areas of the Hat2 β-propeller structure are designated ventral and dorsal sides, respectively, and the outer perimeter is denoted as the side. The rest of the structure is displayed the same as in the *left* panel. (*B*) A view of the structure from the direction facing the ventral side of Hat2. The *left* and *right* panels depict the structure in the same manner as the corresponding panels in *A*, respectively. Each of the seven blades of the Hat2 WD40 propeller structure is labeled. Within each blade, β strands are labeled from 1 to 4, as shown for blade 2.

At the wider end of the H4 tail-binding cleft, a helical turn at the tip of LP2 forms a negatively charged isle, and the C-terminal portion of the H4 tail goes around the isle (Fig. 1). As a consequence, the histone fold core of the H3–H4 heterodimer is snugged into the wedge formed between the C-terminal α-helical module of Hat1 and the dorsal edge of the β propeller near the seventh blade and the very C-terminal of the tail of Hat2 (Fig. 1B). The histone fold domains of both H3 and H4 contact the C-terminal α-helical module of Hat1. Furthermore, the N-terminal portion of H3, from the tail region to α1, interacts with Hat2. H3 residues 1–14 bind the ventral surface of the β propeller, followed by a disordered segment encompassing residues 15–51; residues 52–57 run antiparallel to the outermost strand of the seventh blade and go underneath the N-terminal helix (αN) of Hat2 to join the histone fold domain of H3 (Fig. 1). Histone chaperone Asf1 binds H3–H4 in the same manner as in the stand-alone Asf1–H3–H4 complex (English et al. 2006; Zhang et al. 2018), and the interface between Asf1 and the histone heterodimer faces away from the HAT

complex (Fig. 1). No apparent contact between Asf1 and Hat1–Hat2 was observed, which is consistent with the report that Asf1 binding does not impact the enzymatic activity of the Hat1–Hat2 complex (Haigney et al. 2015).

Structure comparison

Besides the apo structure of yeast Hat1 mentioned earlier, the structures of human Hat1 in complex with an N-terminal peptide of histone H4 as well as yeast Hat1–Hat2 in complex with H3 and H4 peptides have been solved (Wu et al. 2012; Li et al. 2014). The catalytic subunit Hat1 from this study superimposes well with that of human Hat1 and the histone peptide complex of yeast Hat1–Hat2, with RMSDs of 1.1 and 0.4 Å, respectively. As a result of Hat1 superposition, histone H4 residues from Lys8 to Arg17 in all three structures are aligned extremely well (Supplemental Fig. S2A,B), indicating the conserved H4K12 substrate specificity of Hat1 proteins.

The previous structure of the yeast Hat1–Hat2–histone peptide complex was solved using a histone H4 peptide spanning residues 1–48 and a H3 peptide encompassing residues 1–15 (Li et al. 2014). The ordered regions of these peptides contain residues 7–46 of H4 and residues 1–12 of H3. Significant differences from the current Hat1–Hat2–Asf1–H3–H4 structure occur at the H4 region encompassing residues 20–45 (Fig. 2A). H4 residues 30–40 form a helix in both structures, and this helix, known as α1, is part of the conserved histone fold domain. In the complex structure with histone peptides, α1 of H4 is snugly fitted into a cleft in Hat2 formed by LP2 and αN (Fig. 2A; Supplemental Fig. S2B). This H4 binding mode of Hat2 has also been observed in the structures of its metazoan orthologs, human RbAp46/48 and *Drosophila* p55, in complex with short histone H4 fragments encompassing α1 (Supplemental Fig. S3; Murzina et al. 2008; Song et al. 2008). However, in the context of the H3–H4 heterodimer or tetramer, α1 is tightly packed against the central helix, α2, in the core histone fold domains of both H3 and H4. In particular, hydrophobic residues Ile29, Ile34, Leu37, and Ala38, located on or near α1 of H4, interact with αN of Hat2 in the histone peptide complex (Supplemental Fig. S4A), but these residues are buried in interactions with α2 of H4 and H3 (Supplemental Fig. S4B). Furthermore, mutations of Hat2 residues Asn20, Leu23, and M24, seen interacting with H4 α1, resulted in no noticeable effect on the catalytic efficiency of the enzyme complex toward H3–H4 (Haigney et al. 2015). These observations strongly suggest that H4 α1 does not bind Hat2 in this manner in the context of the full-length histone. Indeed, α1 of H4 in our Hat1–Hat2–Asf1–H3–H4 structure points away and makes no contact with Hat2 or Hat1 (Fig. 2A; Supplemental Fig. S2B). This difference in the positioning of the α1 helix results in a large displacement, in the range of 2.7–14 Å, of the H4 loop segment spanning residues 20–30 in the two structures, with the loop segment in the Asf1 complex located closer to LP2 of Hat2 (Fig. 2A).

In the present structure, residues 1–10 of H3 bind the ventral surface of Hat2 similar to that in the structure with the histone H3 peptide (Fig. 1). However, Thr11 begins to make a U-turn, and continuous main chain density ends at Lys14. There are no densities accounting for residues 15–51 of H3 in our structure, but continuous densities for residues 52–134 are unambiguous (Fig. 2B). In this binding manner, residues 52–55 of histone H3 form

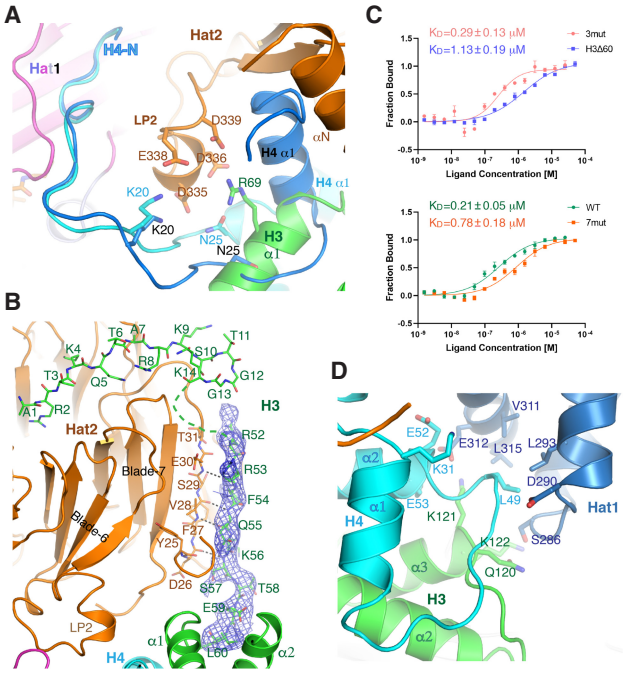

Figure 2. Distinct interactions between Hat1–Hat2 and histones. (*A*) Histone H4 and H3 residues interacting with the LP2 element of Hat2. A histone H4 peptide, colored marine, from PDB structure 4PSX, is superimposed. The involved residues are shown in a stick model. (*B*) Residues 1–14 of H3 bind the ventral surface of Hat2 similar to that in the PDB structure 4PSX, and H3 residues 52–57 adopt an extended conformation and pack against β4 in blade 7. These residues are shown in a stick model, and a section of the simulated annealing Fo–Fc map, contoured at 2σ, with residues 52–60 of H3 omitted, is superimposed. (*C*) K_D values of wild-type (WT); the H4 K20A, N25A, and H3 R69A mutant (3mut); the H3 Q120A, K121A, and K122A and H4 K31A, L49R, E52A and E53A mutant (7mut); and the H3 N-terminal 60-residue deletion (H3Δ60) mutant complexes bound to Hat1–Hat2 measured by MST at 500 mM NaCl. (*D*) Interaction of histone H3 and H4 residues with the α-helical module of the Hat1 C-terminal domain. Involved residues are shown in a stick model.

an antiparallel β-sheet-like interaction with the outermost strand (β4) of Hat2's seventh blade (Fig. 2B).

HAT–histone interaction and impacts on HAT activity

Besides the above-described interactions between histone tails and Hat1–Hat2, additional interactions between Hat1–Hat2 and H3–H4 are concentrated in two regions. The first region surrounds Hat2's LP2 element, where H4 residues 20–25 and Arg69 of H3 are located nearby. However, despite the presence of well-defined, continuous main chain electron density, the density for the side chains of these residues is mostly lacking (Supplemental Fig. S5). Apart from Asn25 of H4, the side chains of H4 Lys20 and H3 Arg69 are inferred to be in the vicinity of LP2 (Fig. 2A). To verify that these histone residues are involved in binding Hat1–Hat2, we made alanine substitutions of all three residues (H3 R69A and H4 K20A N25A), termed 3mut, and measured their binding to Hat1–Hat2 by microscale thermophoresis (MST) (Fig. 2C). In parallel, we also measured the binding of wild-type (WT) histones as well as a combination of N-terminal 60-deletion mutant of H3 (H3Δ60) with full-length H4, all

in the presence of *Af*Asf1. All MST experiments were performed at 500 mM NaCl in order to be able to measure all samples at the same condition, because deletion of N-terminal 60 residues of H3 outcompeted the benefit introduced by *Af*Asf1 and rendered *Af*Asf1–H3Δ60–H4 easily precipitated at a lower salt concentration. Under this condition, Asf1–H3–H4 exhibits a K_D value of 0.21 μM, while the K_D values for the H3–H4 3mut and H3Δ60–H4 mutant complexes with Asf1 are 0.29 μM and 1.13 μM, respectively (Fig. 3C). The result shows that, while Lys20 and Asn25 of H4 and Arg69 of H3 are engaged in interaction with LP2 of Hat2, its role in binding Hat2 is much less significant than that of the N-terminal tail of H3.

The second additional interaction interface occurs between the C-terminal α-helical module of Hat1 and N-terminal portions of α2 of H4 and α3 of H3. A total of seven involved histone residues can be identified. They include Gln120, Lys121, and Lys122 of histone H3, and Lys31, Leu49, Glu52, and Glu53 of H4 (Fig. 2D). However, substitution of all seven residues (7mut) only mildly affected the binding affinities with Hat1–Hat2 (Fig. 2C), suggesting that the contact between Hat1 and histone H3–H4 in this region is not sensitive to the identity of these residues. Likewise, replacing Asp290 and Leu293, two residues in the C-terminal module of Hat1 that are involved in the interaction with H4 residues located in the loop connecting α1 and α2, including Leu49, to alanines resulted in no detectable changes in the binding affinity, whether using the WT or the Asf1–H3Δ60–H4 complex as the substrate (Supplemental Fig. S6A). These results indicate that, outside of the H4 N-terminal recognition sequence, which spans residues 8–17, by the catalytic module of Hat1, the N-terminal tail of H3 contributed the most to the binding affinity between Hat1–Hat2 and histones H3 and H4 in the presence of Asf1. The folded domains of H3 and H4 do not significantly contribute to the binding affinity, although it appears that surface shape complementarity allows comfortable docking of the core domain of histones in the wedge formed by Hat1 and Hat2.

To evaluate the importance of the aforementioned HAT–histone interactions on H4 acetylation, we first assessed the impact of the relevant histone mutations by Western blot. The result shows that the combined triple mutant of R69A of H3 and K20A and N25A of H4 (3mut) affects the H4 acetylation the most, followed by the 7mut of H3 and H4 and H3Δ60 mutant, in an order opposite to their effects in binding Hat1–Hat2 (Fig. 3A). Similar to the 7mut result, Hat1 D290A L293A double mutation reduced the H4 acetylation level to ~70% of that with the WT enzyme, regardless of whether WT or H3Δ60 substrate complexes are used (Supplemental Fig. S6B). Next, we also measured enzyme kinetics of these mutant substrates and compared them with that of the wild-type substrate complex (Fig. 3B). The H3–H4 3mut shows a K_{cat}/K_m value of 1.7 $\mu M^{-1}min^{-1}$ versus 5 $\mu M^{-1}min^{-1}$ for the wild-type Asf1–H3–H4 complex (Fig. 3B). The reduction of acetylation activity toward 3mut comes mostly from H4 mutations, as the substrate complex carrying the H3 R69A mutation alone displays a milder effect compared with the double mutant of H4 (Fig. 3B). The H3–H4 7mut only has a mild effect, at a degree similar to the R69A mutation of H3 alone. Interestingly, the Asf1–H3Δ60–H4 mutant, which has the biggest effect in Hat1–Hat2 binding, showed an activity level comparable with the wild-type substrate complex (Fig. 3B). It should be pointed out that, for the reason pointed out earlier, the enzymatic activity toward the Asf1–H3Δ60–H4 complex was compared with that of the wild-type substrate complex, all measured at 500 mM NaCl. These results indicate that deletion of the N-terminal tail of H3 only affects binding to Hat1–Hat2, but not the enzymatic activity.

In this study, we found a new binding mode between Hat1–Hat2 and histones H3 and H4 in the Asf1–H3–H4 complex. Because Hat2/RbAp46/48 is present in many chromatin-associated complexes, a proper understanding of its histone binding mode is instrumental for dissecting its molecular functions in these complexes. We also noticed an interesting phenomenon in which the substrate binding affinity and the enzymatic activity of the HAT complex are not strictly coupled, as shown most prominently with the H3Δ60 complex. We postulate that there may be two classes of HAT–histone interactions: One class is important for the enzymatic activity and the other is not, but possibly is relevant to nonenzymatic functions of the HAT complex. The interactions between Hat1 and the N-terminal substrate recognition sequence of H4, as well as that between Hat2 LP2 and its binding region in H4, may be grouped into the first class. The interaction between the N-terminal tail of H3 and Hat2 falls into the second class, but what might be the nonenzymatic function of the Hat1–Hat2 complex?

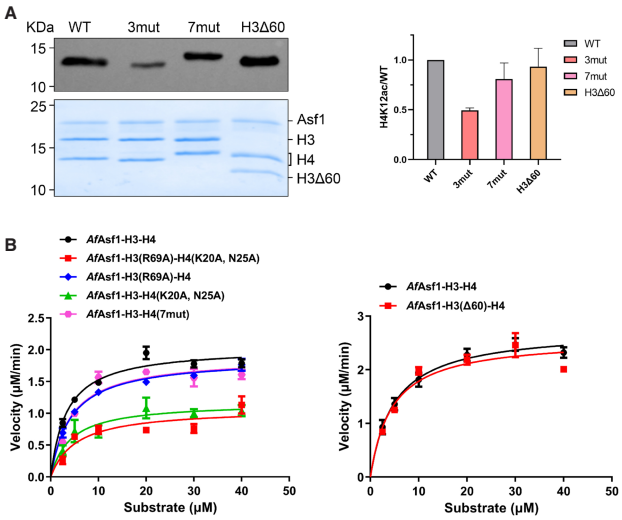

Summary of kinetic parameters

Substrate	K_m (μM)	K_{cat} (min^{-1})	K_{cat}/K_m ($\mu M^{-1}min^{-1}$)
Measured at 150 mM NaCl			
*Af*Asf1-H3-H4	3.4±0.5	17.0±0.6	5.0±0.9
*Af*Asf1-H3-H4(7mut)	4.2±0.9	15.7±0.9	3.7±1.1
*Af*Asf1-H3-H4(3mut)	5.3±2.0	9.0±1.0	1.7±0.9
*Af*Asf1-H3(R69A)-H4	4.2±0.5	15.6±0.5	3.7±0.6
*Af*Asf1-H3-H4(K20A, N25A)	4.1±1.6	9.8±0.9	2.4±1.2
Measured at 500 mM NaCl			
*Af*Asf1-H3-H4	5.0±0.8	23.0±1.0	4.6±1.0
*Af*Asf1-H3(Δ1-60)-H4	4.5±1.0	21.6±1.2	4.8±1.4

Figure 3. Enzymatic activity assays. (*A*, *left* panel) Western blot detection of histone H4 acetylation with wild-type (WT) and mutant Asf1–H3–H4 complexes. (*Right* panel) Quantification of the blots from three independent experiments. The average intensity for the WT substrate is set to unity. (*B*) Michaelis–Menten enzyme kinetic analysis of 125 nM Hat1–Hat2 with the indicated WT and mutant substrate complexes. (*Top left* panel) Results from assays performed at 150 mM NaCl. (*Top right* panel) Results from assays performed at 500 mM NaCl. (*Bottom* panel) Tabulation of enzyme kinetic parameters. A substrate concentration range between 2.5 and 40 μM was used for all experiments.

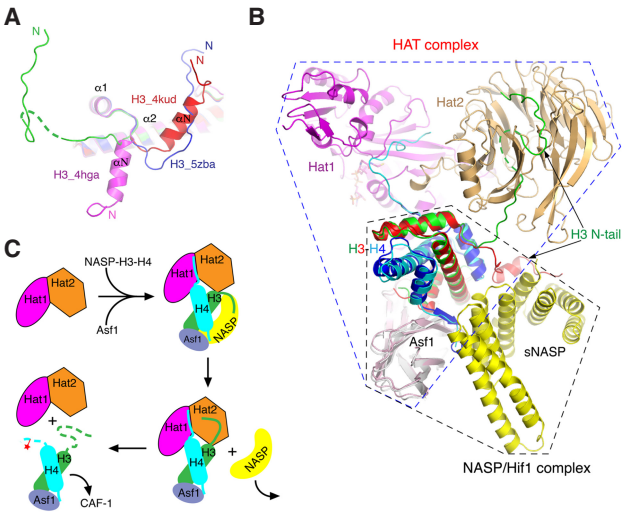

Figure 4. Conformation dynamics of the N-terminal tail of histone H3. (*A*) Residues 45–56 form an α helix, αN, in the nucleosome (PDB ID: 4KUD; colored red). In the DAXX–H3.3–H4 structure (PDB ID: 4HGA; colored magenta), αN, spanning residues 48–59, is oriented nearly opposite to the nucleosomal H3 helix. The H3 regions in the RTT109 complex (PDB ID: 5ZBA; colored blue) and in the present structure (green) are in distinct extended conformations. (*B*) A model of the Hat1–Hat2–H3–H4–Asf1–hif1/sNASP complex assembled by superimposing the Asf1–H3–H4 module in the present structure (enclosed in the blue dashed line hexagon) with that of the sNASP–H3–H4–ASF1 structure (PDB ID: 7V6Q; enclosed in the black dashed line hexagon). The two distinct conformations of the H3 tail are indicated by black arrows. (*C*) A schematic model for transfer of H3–H4 between histone chaperones NASP/Hif1 and Asf1.

The conformational dynamics of the N-terminal tail of H3 offers some insights into the possible nonenzymatic function of the HAT complex. The H3 region spanning residues 52–60 displays drastically different conformation in different complexes (Fig. 4A; Luger et al. 1997; Liu et al. 2012; Zhang et al. 2018). We recently solved a structure of the mammalian sNASP–ASF1–H3–H4 complex (Bao et al. 2021; Liu et al. 2021), which corresponds to a Hif1–Asf1–H3–H4 complex in yeast. This chaperone–histone complex forms a larger complex with HAT1–HAT2 for maintaining a reservoir of soluble histones and facilitating their nuclear import (Campos et al. 2010; Cook et al. 2011). The latter process involves the transfer of histones H3–H4 from sNASP to ASF1, but the mechanism remains unknown. The N-terminal tail of H3 is essential for binding sNASP when ASF1 is present (Liu et al. 2021). Superimposing the two structures via the common Asf1–H3–H4 module revealed a major conformational difference from the N-terminal tail of H3 (Fig. 4B). A possible scenario of handover of H3–H4 from Hif1/sNASP to Asf1 via the conformational switch of the N-terminal tail of H3 is schematically depicted in Figure 4C.

Materials and methods

Protein expression, purification, and crystallization

A large, functional fragment of yeast Hat1 (Hat1ΔC, residues 1–320) was expressed as a 6xHis-tagged or a thermostable cytochrome b_{562}RIL (BRIL) fused protein in *E. coli* using a pCDFDuet-1 or a pRSFDuet-1 vector (Novagen), respectively. Full-length yeast Hat2 was expressed in Sf21 insect cells using the Bac-to-Bac baculovirus expression system (Invitrogen) following the manufacturer's protocol. Hat1–Hat2 complexes were prepared by rupturing Hat1-expressing bacterial cells and Hat2-expressing insect cells together, followed by purification through Ni-NTA and anion exchange column chromatography steps. Asf1–H3–H4 complexes using yeast H3 and H4 or their mutants were assembled with the conserved domain of *S. cerevisiae* or *A. fumigatus* Asf1 (residues 1–154 of both proteins) following a previously described procedure (Zhang et al. 2018). The BRIL–Hat1–Hat2–*Af*Asf1–H3–H4 complex used for crystallization was assembled by mixing purified subcomplexes at an ~1:1 molar ratio and purifying them again through a sizing column. Best diffracting crystals were grown with ~15 mg/mL protein complex and 0.6 mM CoA at 16°C in a condition with 100 mM Bis-Tris propane (pH 6.5), 20% (v/v) PEG-3350, and 200 mM sodium nitrate. Detailed procedures are described in the Supplemental Material.

Crystallographic data collection and structure determination

X-ray diffraction data were collected at beamline BL17U1 of the Shanghai Synchrotron Radiation Facility (SSRF) at a wavelength of 0.9792 Å, and the structure was solved by molecular replacement using the Hat1–Hat2–H4 peptide complex structure (PDB: 4PSW) as the search model. Structure refinements were performed with two group B factors—one for main chain and another for side chain atoms of each residue—due to the limitation of a low number of reflections. Statistics of data collection and refinement are shown in Supplemental Table S1. Atomic coordinates and structure factors have been deposited in PDB under accession number 7XAY. Detailed procedures are described in the Supplemental Material.

HAT assay

Western blot analysis of HAT activities was performed with an antibody against acetyl-lysine 5 and/or 12 of histone H4 (1:2000 dilution; Abcam ab177790) and detected by the Enhanced ECL luminescence detection kit (Thermo 34577). Three independent blots were quantified by image scanning to derive the error bars. Quantitative HAT activity analyses used a continuous fluorometric HAT assay (Chung et al. 2008). The data were first analyzed using Excel and then fitted to the Michaelis–Menten equation using GraphPad Prism (GraphPad Software, Inc.). The K_m and K_{cat} values were derived by varying the concentration of the substrate. Detailed conditions for the assay are described in the Supplemental Material.

Microscale thermophoresis (MST) analysis

MST measurements of binding affinities were performed using a Monolith NT.115 instrument (NanoTemper) and premium glass capillary tubes (NanoTemper MO-K025). All measurements were performed in triplicate, and the thermophoresis data were analyzed with the MO affinity analysis software (NanoTemper) or GraphPad Prism 8. Detailed procedures are described in the Supplemental Material.

Competing interest statement

The authors declare no competing interests.

Acknowledgments

We thank Chunyu Wang for providing the BRIL expression plasmid, staff scientists at Shanghai Synchrotron Radiation Facility beamline BL17U1 and Yi Han at the Institute of Biophysics core facility for assistance with X-ray data collection; Yuanyuan Chen, Zhenwei Yang, and Bingxue Zhou for technical help with the MST assay; Dr. Na Yang for helpful discussions; and Jingjing Chen for help with logistics. This work was supported in part by grants from the Natural Science Foundation of China (91853204, 92153302, 31991162, and 31521002), the Ministry of Science and Technology of China (2019YFA0508900 and 2018YFE0203300), and the Strategic Priority Research Program of Chinese Academy of Sciences (CAS; XDB37010101). C.P.L. is supported by the Youth Innovation Promotion Association of the CAS (2018125).

Author contributions: R.-M.X conceived the project and supervised the study. Y.Y. carried out protein expression, purification, crystallization, mutagenesis, and enzymatic analyses. W.-S.Y. performed structure determination and refinement, and analyzed enzyme–substrate interactions and enzymatic activities. L.Z. performed protein expression and purification at an early stage of the work. C.-P.L. helped with structure determination. Y.Y., W.-S.Y., and R.-M.X. wrote the manuscript, and all authors read and edited the manuscript.

References

Ai X, Parthun MR. 2004. The nuclear Hat1p/Hat2p complex: a molecular link between type B histone acetyltransferases and chromatin assembly. *Mol Cell* **14:** 195–205. doi:10.1016/S1097-2765(04)00184-4

Alvarez F, Muñoz F, Schilcher P, Imhof A, Almouzni G, Loyola A. 2011. Sequential establishment of marks on soluble histones H3 and H4. *J Biol Chem* **286:** 17714–17721. doi:10.1074/jbc.M111.223453

Bao H, Carraro M, Flury V, Liu Y, Luo M, Chen L, Groth A, Huang H. 2021. NASP maintains histone H3–H4 homeostasis through two distinct H3 binding modes. bioRxiv doi:10.1101/2021.1102.467034

Berndsen CE, Denu JM. 2008. Catalysis and substrate selection by histone/protein lysine acetyltransferases. *Curr Opin Struct Biol* **18:** 682–689. doi:10.1016/j.sbi.2008.11.004

Brownell JE, Zhou J, Ranalli T, Kobayashi R, Edmondson DG, Roth SY, Allis CD. 1996. Tetrahymena histone acetyltransferase A: a homolog to yeast Gcn5p linking histone acetylation to gene activation. *Cell* **84:** 843–851. doi:10.1016/S0092-8674(00)81063-6

Campos EI, Fillingham J, Li G, Zheng H, Voigt P, Kuo WH, Seepany H, Gao Z, Day LA, Greenblatt JF, et al. 2010. The program for processing newly synthesized histones H3.1 and H4. *Nat Struct Mol Biol* **17:** 1343–1351. doi:10.1038/nsmb.1911

Chun E, Thompson AA, Liu W, Roth CB, Griffith MT, Katritch V, Kunken J, Xu F, Cherezov V, Hanson MA, et al. 2012. Fusion partner toolchest for the stabilization and crystallization of G protein-coupled receptors. *Structure* **20:** 967–976. doi:10.1016/j.str.2012.04.010

Chung CC, Ohwaki K, Schneeweis JE, Stec E, Varnerin JP, Goudreau PN, Chang A, Cassaday J, Yang L, Yamakawa T, et al. 2008. A fluorescence-based thiol quantification assay for ultra-high-throughput screening for inhibitors of coenzyme A production. *Assay Drug Dev Technol* **6:** 361–374. doi:10.1089/adt.2007.105

Cook AJ, Gurard-Levin ZA, Vassias I, Almouzni G. 2011. A specific function for the histone chaperone NASP to fine-tune a reservoir of soluble H3–H4 in the histone supply chain. *Mol Cell* **44:** 918–927. doi:10.1016/j.molcel.2011.11.021

Driscoll R, Hudson A, Jackson SP. 2007. Yeast Rtt109 promotes genome stability by acetylating histone H3 on lysine 56. *Science* **315:** 649–652. doi:10.1126/science.1135862

Dutnall RN, Tafrov ST, Sternglanz R, Ramakrishnan V. 1998. Structure of the histone acetyltransferase Hat1: a paradigm for the GCN5-related N-acetyltransferase superfamily. *Cell* **94:** 427–438. doi:10.1016/S0092-8674(00)81584-6

English CM, Adkins MW, Carson JJ, Churchill ME, Tyler JK. 2006. Structural basis for the histone chaperone activity of Asf1. *Cell* **127:** 495–508. doi:10.1016/j.cell.2006.08.047

Grant PA, Duggan L, Côté J, Roberts SM, Brownell JE, Candau R, Ohba R, Owen-Hughes T, Allis CD, Winston F, et al. 1997. Yeast Gcn5 functions in two multisubunit complexes to acetylate nucleosomal histones: characterization of an Ada complex and the SAGA (Spt/Ada) complex. *Genes Dev* **11:** 1640–1650. doi:10.1101/gad.11.13.1640

Haigney A, Ricketts MD, Marmorstein R. 2015. Dissecting the molecular roles of histone chaperones in histone acetylation by type B histone acetyltransferases (HAT-B). *J Biol Chem* **290:** 30648–30657. doi:10.1074/jbc.M115.688523

Han J, Zhou H, Horazdovsky B, Zhang K, Xu RM, Zhang Z. 2007. Rtt109 acetylates histone H3 lysine 56 and functions in DNA replication. *Science* **315:** 653–655. doi:10.1126/science.1133234

Kleff S, Andrulis ED, Anderson CW, Sternglanz R. 1995. Identification of a gene encoding a yeast histone H4 acetyltransferase. *J Biol Chem* **270:** 24674–24677. doi:10.1074/jbc.270.42.24674

Li Y, Zhang L, Liu T, Chai C, Fang Q, Wu H, Agudelo Garcia PA, Han Z, Zong S, Yu Y, et al. 2014. Hat2p recognizes the histone H3 tail to specify the acetylation of the newly synthesized H3/H4 heterodimer by the Hat1p/Hat2p complex. *Genes Dev* **28:** 1217–1227. doi:10.1101/gad.240531.114

Liu CP, Xiong C, Wang M, Yu Z, Yang N, Chen P, Zhang Z, Li G, Xu RM. 2012. Structure of the variant histone H3.3–H4 heterodimer in complex with its chaperone DAXX. *Nat Struct Mol Biol* **19:** 1287–1292. doi:10.1038/nsmb.2439

Liu CP, Jin W, Hu J, Wang M, Chen J, Li G, Xu RM. 2021. Distinct histone H3-H4 binding modes of sNASP reveal the basis for cooperation and competition of histone chaperones. *Genes Dev* **35:** 1610–1624. doi:10.1101/gad.349100.121

Luger K, Mäder AW, Richmond RK, Sargent DF, Richmond TJ. 1997. Crystal structure of the nucleosome core particle at 2.8 A resolution. *Nature* **389:** 251–260. doi:10.1038/38444

Marmorstein R, Trievel RC. 2009. Histone modifying enzymes: structures, mechanisms, and specificities. *Biochim Biophys Acta* **1789:** 58–68. doi:10.1016/j.bbagrm.2008.07.009

Mousson F, Ochsenbein F, Mann C. 2007. The histone chaperone Asf1 at the crossroads of chromatin and DNA checkpoint pathways. *Chromosoma* **116:** 79–93. doi:10.1007/s00412-006-0087-z

Murzina NV, Pei XY, Zhang W, Sparkes M, Vicente-Garcia J, Pratap JV, McLaughlin SH, Ben-Shahar TR, Verreault A, Luisi BF, et al. 2008. Structural basis for the recognition of histone H4 by the histone-chaperone RbAp46. *Structure* **16:** 1077–1085. doi:10.1016/j.str.2008.05.006

Parthun MR, Widom J, Gottschling DE. 1996. The major cytoplasmic histone acetyltransferase in yeast: links to chromatin replication and histone metabolism. *Cell* **87:** 85–94. doi:10.1016/S0092-8674(00)81325-2

Poveda A, Pamblanco M, Tafrov S, Tordera V, Sternglanz R, Sendra R. 2004. Hif1 is a component of yeast histone acetyltransferase B, a complex mainly localized in the nucleus. *J Biol Chem* **279:** 16033–16043. doi:10.1074/jbc.M314228200

Qian YW, Wang YC, Hollingsworth RE Jr, Jones D, Ling N, Lee EY. 1993. A retinoblastoma-binding protein related to a negative regulator of Ras in yeast. *Nature* **364:** 648–652. doi:10.1038/364648a0

Qin S, Parthun MR. 2002. Histone H3 and the histone acetyltransferase Hat1p contribute to DNA double-strand break repair. *Mol Cell Biol* **22:** 8353–8365. doi:10.1128/MCB.22.23.8353-8365.2002

Roth SY, Denu JM, Allis CD. 2001. Histone acetyltransferases. *Annu Rev Biochem* **70:** 81–120. doi:10.1146/annurev.biochem.70.1.81

Ruiz-García AB, Sendra R, Galiana M, Pamblanco M, Pérez-Ortı´n JE, Tordera V. 1998. HAT1 and HAT2 proteins are components of a yeast nuclear histone acetyltransferase enzyme specific for free histone H4. *J Biol Chem* **273:** 12599–12605. doi:10.1074/jbc.273.20.12599

Soffers JHM, Workman JL. 2020. The SAGA chromatin-modifying complex: the sum of its parts is greater than the whole. *Genes Dev* **34:** 1287–1303. doi:10.1101/gad.341156.120

Song JJ, Garlick JD, Kingston RE. 2008. Structural basis of histone H4 recognition by p55. *Genes Dev* **22:** 1313–1318. doi:10.1101/gad.1653308

Sterner DE, Wang X, Bloom MH, Simon GM, Berger SL. 2002. The SANT domain of Ada2 is required for normal acetylation of histones by the yeast SAGA complex. *J Biol Chem* **277:** 8178–8186. doi:10.1074/jbc.M108601200

Tyler JK, Adams CR, Chen SR, Kobayashi R, Kamakaka RT, Kadonaga JT. 1999. The RCAF complex mediates chromatin assembly during DNA replication and repair. *Nature* **402:** 555–560. doi:10.1038/990147

Verreault A, Kaufman PD, Kobayashi R, Stillman B. 1998. Nucleosomal DNA regulates the core-histone-binding subunit of the human Hat1 acetyltransferase. *Curr Biol* **8:** 96–108. doi:10.1016/S0960-9822(98)70040-5

Wang H, Dienemann C, Stützer A, Urlaub H, Cheung ACM, Cramer P. 2020. Structure of the transcription coactivator SAGA. *Nature* **577:** 717–720. doi:10.1038/s41586-020-1933-5

Wu H, Moshkina N, Min J, Zeng H, Joshua J, Zhou MM, Plotnikov AN. 2012. Structural basis for substrate specificity and catalysis of human histone acetyltransferase 1. *Proc Natl Acad Sci* **109:** 8925–8930. doi:10.1073/pnas.1114117109

Zhang L, Serra-Cardona A, Zhou H, Wang M, Yang N, Zhang Z, Xu RM. 2018. Multisite substrate recognition in Asf1-dependent acetylation of histone H3 K56 by Rtt109. *Cell* **174:** 818–830.e11. doi:10.1016/j.cell.2018.07.005